COMMUNICATION

Spark Ablation: a dry, physical, and continuous method to prepare powdery metal nanoparticle-based catalysts†

Received 00th January 20xx,
Accepted 00th January 20xx

DOI: 10.1039/x0xx00000x

Damien P. Debecker,*[a] Plaifa Hongmanorom,[a] Tobias V. Pfeiffer,[b] Bernardus Zijlstra,[b] Yingrui Zhao,[a] Sandra Casale[c] and Capucine Sassoye[d]

We report the first synthesis of a powdery heterogeneous catalyst using spark ablation technology. A TiO_2 powder is aerosolized in a vortex and injected close to the electrode of a spark ablation nanoparticles generator, to be decorated with Ni nanoparticles. The resulting Ni/TiO_2 catalyst is readily active in the hydrogenation of CO_2 to methane.

Numerous preparation methods have been adopted for the synthesis of metal nanoparticles and supported metal nanoparticles. Wet chemical treatments (e.g. impregnation, grafting, colloidal deposition, etc.) are the most common processes implemented for both lab-scale and industrial-scale production of (supported) nanoparticles.[1, 2] These processes usually involve the use of solvent along with metallic salt or metallic oxide precursors, which inevitably generates large amounts of liquid waste containing solvent, ligand, counter ions, etc.[3-5] Also, these chemical methods mostly rely on time-consuming batch operations and multi-step procedures, such as precursor solution preparation, aging, drying/evaporation, calcination, reduction. Thermal treatment/activation steps in particular are energy-intensive.[6] In addition to environmental and economic challenges, controlling the nanoscale properties of the materials synthesized via wet chemical routes still remains challenging. A tedious fine-tuning of various synthesis parameters (types of metal precursor and solvent, pH, temperature, time, etc.) is required to control the size, shape, and composition (i.e. in alloys) of nanoparticles as well as the interaction between metal and support.[2, 7, 8] It is thus worthwhile to find a greener and simpler synthesis alternative to the preparation of nanoparticles and supported metal nanoparticles with well-defined properties.

Spark ablation was developed to generate nanoparticles,[9] using electrical discharges between two electrodes of a target material in a flow of inert gas. This physical process yields primary metal particles several nanometers in size.[10] It is a compelling alternative to wet chemical methods to metal nanoparticles, primed to reduced environmental impact: it readily leads to clean particles without using solvents, precursors, salts, ligands, or high temperature treatments. Different particles can be readily mixed to form composite nanostructured materials, making it a powerful tool for materials development.[11] The generated particles are often deposited onto flat substrates directly from the aerosol, where they form nanoporous layers for e.g. electrocatalysis,[12] gas sensors,[13, 14] surface-enhanced Raman spectroscopy,[15] etc. Thus, the well-controlled deposition of tailored metal nanoparticles onto flat surfaces has been well documented. Yet, for heterogeneous catalysis, powdery samples are needed.

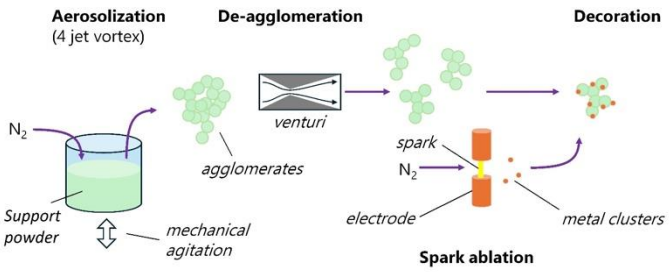

Scheme 1 Schematic view on the set-up used to prepare powdery Ni/TiO_2 catalysts. The support powder is aerosolized using a 4-jet vortex fed with N_2 and gas-transported to be de-agglomerated in a venturi and finally injected in the spark generator. Sparks created between the Ni electrodes create Ni clusters, which aggregate to form Ni nanoparticles deposited onto the TiO_2 particles. The Ni/TiO_2 is collected on a separation filter (see more detailed description in the ESI).

We propose to adapt the spark nanoparticle generator to allow a direct deposition onto pulverulent materials. The concept relies on the aerosolization of a powder which is gas-transported and injected in the path of the metal nanoparticles formation (Scheme 1, and ESI). Here, a TiO_2 powder (Degussa P25) was used as the catalyst support and Ni electrodes were used to form Ni nanoparticles as the active phase.

[a] Institute of Condensed Matter and Nanoscience (IMCN), UCLouvain, 1348 Louvain-La-Neuve, Belgium. E-mail: damien.debecker@uclouvain.be
[b] VSParticle B.V., Oostsingel 209, 2612 HL, Delft, the Netherlands
[c] Laboratoire de Réactivité de Surface (LRS), CNRS, Sorbonne Université, 4 Place Jussieu, 75005, Paris, France
[d] Laboratoire de Chimie de la Matière Condensée de Paris (LCMCP), College de France, Sorbonne Université, CNRS, 4 Place Jussieu, 75005 Paris, France

† Electronic Supplementary Information (ESI) available: Experimental procedure (catalyst synthesis, spark ablation generator, powder disperser, characterization and CO_2 methanation) and comparison of CO_2 conversion rates with the reported catalysts. See DOI: 10.1039/x0xx00000x

Textural properties were analyzed by N_2 physisorption. As shown in Fig. 1a, both TiO_2 and Ni/TiO_2 exhibit a H3-type hysteresis loop resulting from the interparticle voids in the loose aggregates of non-porous TiO_2 particles.[16, 17] In the literature, the P25 TiO_2 materials in general show decreased specific surface area and increased average pore diameter after the metal loading and/or thermal treatment due to the sintering of TiO_2 crystallites,[18, 19] which is not the case here. Compared with the pristine TiO_2 support in Table 1, the Ni/TiO_2 catalyst has higher specific surface area, indicating the absence of TiO_2 sintering. The total pore volume increased slightly (especially small pores of 2 nm, as presented in Fig. 1b). It was also reported that the average pore diameter corresponds to the TiO_2 crystallite size.[20] A decrease in the average pore diameter of the Ni/TiO_2 catalyst thus could be due to the presence of small Ni crystallites over TiO_2 support.

The diffractograms of the P25 TiO_2 support, fresh, and spent Ni/TiO_2 catalysts are presented in Fig. 2a. This commercial TiO_2 powder is marketed with a rutile content of 15-25 wt.% and 75-85 wt.% of anatase.[18, 21, 22] After nickel loading and CO_2 methanation reaction, the TiO_2 diffraction peaks are unchanged in intensity, positions and width, which suggests that TiO_2 crystallites are unaffected by the catalyst preparation and reaction conditions. Additionally, the main diffraction peaks of Ni (2θ = 44.6°) or NiO (2θ = 43.1°) crystalline phases are not detectable in the XRD pattern of the as-prepared Ni/TiO_2 catalyst, excluding the presence of Ni-based crystallites larger than 5 nm.[23] In contrast, a small diffraction peak is detected at 44.6° for the spent catalyst (Fig. 2a, top) attesting the presence of few larger metallic Ni particles. Scherrer calculation on this unique peak allows evaluating a mean particle size of 52 nm.

Table 1. Textural properties of TiO_2 support, fresh Ni/TiO_2 catalyst and spent Ni/TiO_2 catalyst.

Sample	BET surface area (m^2/g)	Total pore volume (cm^3/g)	Average Pore diameter (nm)
TiO_2	50	0.20	16
Ni/TiO_2	78	0.22	14

The H_2-TPR profile depicted in Fig. 2b shows the reducibility of the as-prepared Ni/TiO_2 catalyst. The main peak observed at 295 °C likely corresponds to the reduction of NiO weakly interacting with TiO_2, while the shoulder peak spanning from 350 °C to 450 °C could indicate the reduction of NiO having a stronger interaction with TiO_2.[24, 25] The amount of H_2 consumed is 0.26 mmol/g_{cat}, which is lower than the corresponding Ni loading 0.39 mmol/g_{cat} (2.3 wt%) determined by ICP-AES. It is worth noting that, theoretically and feasibly, fully reduced metal particles are produced from the spark ablation of metal electrodes under inert gas environment.[11] The detection of a H_2 consumption in TPR points to the presence of NiO. This must be related to the (well-known) passivation of Ni metal, likely during the storage and handling of the sample in ambient conditions. To prevent such oxidation, oxygen-free environment could be applied for preparation, handling, and storage in future studies.

The overall morphology of the as-prepared Ni/TiO_2 catalyst is revealed in TEM (Fig. 3a). Many small Ni nanoparticles (<5 nm, see blue arrows) are well-dispersed on TiO_2. HRTEM images in Fig. 3b and 3c display lattice fringes with inter-planar distances of 2.0-2.1 Å and 2.35-2.45 Å. The former interatomic distance corresponds to the (111) crystal plane of cubic Ni, while the latter is attributed to the (111) crystal plane of cubic NiO.[26, 27] Cubic NiO crystallites could stem from the full oxidation of ultrafine particles (≤ 3 nm) during sample storage or handling. For larger particles (> 3 nm), a superficial oxide layer could be formed on the metal particles.[10, 28] It should be noted that the homogeneity of the deposit is not optimal. As shown in Fig. 3(d), some "floating" Ni/NiO nanoparticles can also be observed, not being in contact with the TiO_2 support. Despite no interaction with TiO_2 support, these nanoparticles are very small, which is consistent with the absence of Ni or NiO crystallites in the XRD pattern of the as-prepared catalyst in Fig. 2(a).

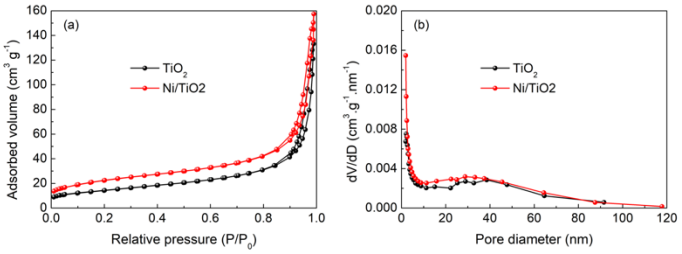

Fig. 1 (a) N_2 adsorption-desorption isotherms and (b) pore size distribution obtained via

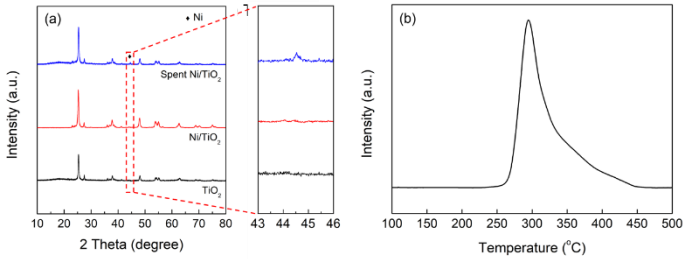

Fig. 2 (a) XRD patterns of TiO_2 support, fresh Ni/TiO_2 catalyst and spent Ni/TiO_2 catalyst. (b) H_2-TPR profile of Ni/TiO_2 catalyst.

As commonly done for Ni-based catalysts (to counter surface passivation), the catalyst was in-situ reduced under H_2/He at 500 °C prior to being tested in CO_2 methanation reaction from 200 °C to 400 °C. The reaction conditions (contact time) were chosen so as to obtain relatively low CO_2 conversion levels, deliberately distancing from the thermodynamic equilibrium and ensuring the measurement of intrinsic activity. The two main products during CO_2 hydrogenation on the Ni/TiO_2 are CH_4 via CO_2 methanation and CO via reverse water-gas shift. The corresponding CH_4 selectivity is shown in Fig. 4, where a maximum CH_4 selectivity of 81% is obtained at 350 °C. Table S1 demonstrates that the spark ablation-produced supported Ni nanoparticle catalyst exhibits comparatively lower selectivity toward CH_4 than several other methanation catalysts reported in the literature. This result could probably be attributed to the small size of most of the Ni nanoparticles in the spark-made Ni/TiO_2 catalyst. Indeed, on the spent catalyst, small Ni nanoparticles stabilized on TiO_2 are visualized in the TEM images (Fig. 5a and 5b). Many studies attribute the relatively low CH_4 selectivity during CO_2 hydrogenation on Ni nanoparticles below 5 nm to low availability of active sites,

particularly step-edge sites for CO dissociation and adjacent adsorbed H sites for further hydrogenation to CH_4.[29-31] A further discussion on the effect of metal-support interaction in these catalysts is presented in ESI. Besides small Ni nanoparticles, few large particles (50-80 nm) can be found in TEM image (Fig. 5c) of the spent Ni/TiO_2 catalyst, likely stemming from the sintering of "floating" Ni nanoparticles without interaction with TiO_2 observed in Fig. 3d. The slow on-stream deactivation observed at 350°C and 400°C may be a further indication of this sintering (Fig. S4). The presence on TEM picture of those few large Ni nanoparticles is consistent with the small and relatively narrow XRD peak at 44.6° (Fig.2, top). There is consensus in the literature on the fact that such large unsupported Ni particles are much less active than small supported Ni particles.[32, 33]

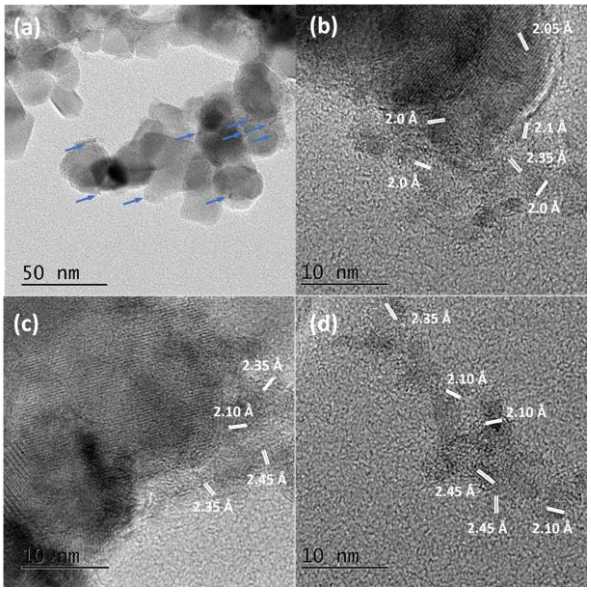

Fig. 3 (a) TEM and (b) and (c) HRTEM images of the as-prepared Ni/TiO_2 catalyst. (d) HRTEM image of "floating" Ni and NiO nanoparticles in the Ni/TiO_2 catalyst.

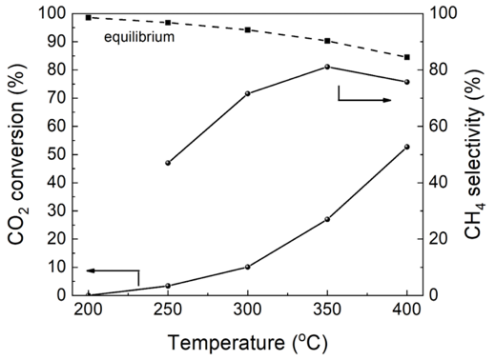

Fig. 4 CO_2 conversion and CH_4 selectivity of the Ni/TiO_2 catalyst as a function of temperature ranging from 200 °C to 400 °C.

Although the Ni loading, Ni particle size and metal-support interaction have not been fine-tuned in this study, the specific activity of the spark-ablated Ni/TiO_2 catalyst in terms of CO_2 conversion rate is comparable to that of some reported Ni catalysts (Table S1).[34-42] Some other optimized Ni catalysts exhibit higher conversion rates, suggesting that there is still room for amelioration. For example, improving the design of the mixing zone could increase the quality of the dispersion of metal NP onto the support (to avoid "floating" NP). We also suggest expanding the scope of investigation (i) to other metals, particularly those in groups 8-10 (e.g., Ru, Rh, Pd, Co and Fe), which have been reported as active and selective metal catalysts for CO_2 methanation, (ii) to alloys (using 2 electrodes made of 2 different metals, or using electrodes made of alloys), and (iii) to vary the size of the metal nanoparticles by adapting the operating conditions of the nanoparticles generator.

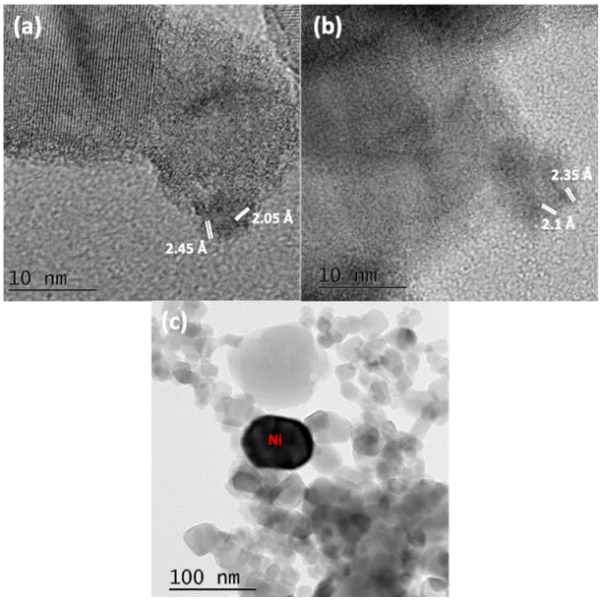

Fig. 5 (a) and (b) HRTEM images of the spent Ni/TiO_2 catalyst and (c) TEM image of large Ni particle without interaction with TiO_2 after CO_2 hydrogenation from 200 °C to 400 °C.

This is the first time that a spark-ablation nanoparticle generator has been coupled with a powder aerosol disperser for the production of supported metal nanoparticle catalysts. As a proof of concept, the Ni/TiO_2 catalyst prepared by this method demonstrated similar activity in CO_2 methanation, compared to other Ni-based catalysts reported in the literature. Small Ni nanoparticles (a few nm), well-dispersed on TiO_2 support, remained stabilized after reductive pretreatment and reaction. Nevertheless, the observation of "floating' Ni nanoparticles indicated that the homogeneity of deposition could be improved. The disclosed preparation method is physical, continuous ligand-less, and solvent-less. It opens new avenues for heterogeneous catalyst preparation, as it offers a straightforward, adaptable, and resource-efficient alternative to classical preparation methods, avoiding the use of expensive precursors, minimizing waste generation, and eliminating energy-demanding drying and calcination steps. It may serve as a new environmentally friendly pathway for heterogeneous catalyst synthesis, aligning with the principles of green chemistry. Future development of this approach should confirm if metal loading, nanoparticle size, and homogeneity of deposition can be tuned by adjusting the parameters of the method, including the flow rates, the settings for the spark

generator and for powder disperser. Exploring various metals and supports, it will be worthwhile to explore if metal-support interactions established via this "clean" preparation show similarities with catalysts prepared with classical methods.

Conflicts of interest

There are no conflicts to declare.

Data availability

The data supporting this article have been included as part of the Supplementary Information.

References

1. K. Liu, X. Zhao, G. Ren, T. Yang, Y. Ren, A. F. Lee, Y. Su, X. Pan, J. Zhang, Z. Chen, J. Yang, X. Liu, T. Zhou, W. Xi, J. Luo, C. Zeng, H. Matsumoto, W. Liu, Q. Jiang, K. Wilson, A. Wang, B. Qiao, W. Li and T. Zhang, *Nature Commun.*, 2020, **11**, 1263.
2. A. V. Nikam, B. L. V. Prasad and A. A. Kulkarni, *CrystEngComm*, 2018, **20**, 5091-5107.
3. C. Sassoye, G. Muller, D. P. Debecker, A. Karelovic, S. Cassaignon, C. Pizarro, P. Ruiz and C. Sanchez, *Green Chem.*, 2011, **13**, 3230-3237.
4. N.-D. Jaji, H. L. Lee, M. H. Hussin, H. M. Akil, M. R. Zakaria and M. B. H. Othman, *Nanotechnol. Rev.*, 2020, **9**, 1456-1480.
5. D. P. Debecker, K. Kuok Hii, A. Moores, L. M. Rossi, B. Sels, D. T. Allen and B. Subramaniam, *ACS Sus. Chem. Eng.*, 2021, **9**, 4936-4940.
6. N. Osterwalder, C. Capello, K. Hungerbühler and W. J. Stark, *J. Nanopart. Res.*, 2006, **8**, 1-9.
7. N. Baig, I. Kammakakam and W. Falath, *Mater. Adv.*, 2021, **2**, 1821-1871.
8. K. Kusada, M. Mukoyoshi, D. Wu and H. Kitagawa, *Angew. Chem. Int. Ed.*, 2022, **61**, e202209616.
9. S. Schwyn, E. Garwin and A. Schmidt-Ott, *J. Aerosol Sci*, 1988, **19**, 639-642.
10. C. Vogt, F. Meirer, M. Monai, E. Groeneveld, D. Ferri, R. A. van Santen, M. Nachtegaal, R. R. Unocic, A. I. Frenkel and B. M. Weckhuysen, *Nature Commun.*, 2021, **12**, 7096.
11. T. V. Pfeiffer, J. Feng and A. Schmidt-Ott, *Adv. Powder Technol.*, 2014, **25**, 56-70.
12. F. M. Sapountzi, M. Lavorenti, W. Vrijburg, S. Dimitriadou, B. Tyburska-Pueschel, P. Thüne, H. Niemantsverdriet, T. V. Pfeiffer and M. N. Tsampas, *Catalysts*, 2022, **12**, 1343.
13. N. A. Isaac, P. Ngene, R. J. Westerwaal, J. Gaury, B. Dam, A. Schmidt-Ott and G. Biskos, *Sensors Actuators B: Chem.*, 2015, **221**, 290-296.
14. N. A. Isaac, M. Valenti, A. Schmidt-Ott and G. Biskos, *ACS Appl. Mater. Interfaces*, 2016, **8**, 3933-3939.
15. S. Aghajani, A. Accardo and M. Tichem, *ACS Appl. Nano Mater.*, 2020, **3**, 5665-5675.
16. M. Thommes, K. Kaneko, A. V. Neimark, J. P. Olivier, F. Rodriguez-Reinoso, J. Rouquerol and K. S. W. Sing, *Pure Appl. Chem.*, 2015, **87**, 1051-1069.
17. H. Hayashi and K. Torii, *J. Mater. Chem.*, 2002, **12**, 3671-3676.
18. G. Wang, L. Xu, J. Zhang, T. Yin and D. Han, *Int. J. Photoenergy*, 2012, **2012**, 265760.
19. A. Kim, C. Sanchez, G. Patriarche, O. Ersen, S. Moldovan, A. Wisnet, C. Sassoye and D. P. Debecker, *Catal. Sci. Technol.*, 2016, **6**, 8117-8128.
20. J. Yu, H. Yu, B. Cheng, M. Zhou and X. Zhao, *J. Mol. Catal. A: Chem.*, 2006, **253**, 112-118.
21. A. M. Pennington, A. I. Okonmah, D. T. Munoz, G. Tsilomelekis and F. E. Celik, *J. Phys. Chem. C*, 2018, **122**, 5093-5104.
22. G. Zhou, R. Dou, H. Bi, S. Xie, Y. Pei, K. Fan, M. Qiao, B. Sun and B. Zong, *J. Catal.*, 2015, **332**, 119-126.
23. P. Hongmanorom, J. Ashok, G. Zhang, Z. Bian, M. H. Wai, Y. Zeng, S. Xi, A. Borgna and S. Kawi, *Appl. Catal., B*, 2021, **282**, 119564.
24. M. Xu, S. He, H. Chen, G. Cui, L. Zheng, B. Wang and M. Wei, *ACS Catal.*, 2017, **7**, 7600-7609.
25. J. Liu, C. Li, F. Wang, S. He, H. Chen, Y. Zhao, M. Wei, D. G. Evans and X. Duan, *Catal. Sci. Technol.*, 2013, **3**, 2627-2633.
26. Y. Yang, X. Sun, G. Han, X. Liu, X. Zhang, Y. Sun, M. Zhang, Z. Cao and Y. Sun, *Angew. Chem. Int. Ed.*, 2019, **58**, 10644-10649.
27. W. Liu, H. Feng, Y. Yang, Y. Niu, L. Wang, P. Yin, S. Hong, B. Zhang, X. Zhang and M. Wei, *Nature Commun.*, 2022, **13**, 3188.
28. Y. Yang, M. Johansson, A. Wiorek, N. V. Tarakina, F. Sayed, R. Mathieu, M. Jonsson and I. L. Soroka, *Dalton Trans.*, 2021, **50**, 376-383.
29. H. C. Wu, Y. C. Chang, J. H. Wu, J. H. Lin, I. K. Lin and C. S. Chen, *Catal. Sci. Technol.*, 2015, **5**, 4154-4163.
30. C. Vogt, E. Groeneveld, G. Kamsma, M. Nachtegaal, L. Lu, C. J. Kiely, P. H. Berben, F. Meirer and B. M. Weckhuysen, *Nature Catal.*, 2018, **1**, 127-134.
31. J. F. M. Simons, T. J. de Heer, R. C. J. van de Poll, V. Muravev, N. Kosinov and E. J. M. Hensen, *J. Am. Chem. Soc.*, 2023, **145**, 20289-20301.
32. G. Varvoutis, M. Lykaki, S. Stefa, V. Binas, G. E. Marnellos and M. Konsolakis, *Appl. Catal., B*, 2021, **297**, 120401.
33. G. Garbarino, P. Riani, L. Magistri and G. Busca, *Int. J. Hydrogen Energy*, 2014, **39**, 11557-11565.
34. P. Unwiset, K. C. Chanapattharapol, P. Kidkhunthod, Y. Poo-arporn and B. Ohtani, *Chem. Eng. Sci.*, 2020, **228**, 115955.
35. Y. Yu, Y. M. Chan, Z. Bian, F. Song, J. Wang, Q. Zhong and S. Kawi, *Int. J. Hydrogen Energy*, 2018, **43**, 15191-15204.
36. F. Song, Q. Zhong, Y. Yu, M. Shi, Y. Wu, J. Hu and Y. Song, *Int. J. Hydrogen Energy*, 2017, **42**, 4174-4183.
37. L. Bian, L. Zhang, R. Xia and Z. Li, *J. Nat. Gas Sci. Eng.*, 2015, **27**, 1189-1194.
38. Q. Liu, S. Wang, G. Zhao, H. Yang, M. Yuan, X. An, H. Zhou, Y. Qiao and Y. Tian, *Int. J. Hydrogen Energy*, 2018, **43**, 239-250.
39. Y. Zhao, V. Girelli, O. Ersen and D. P. Debecker, *J. Catal.*, 2023, **426**, 283-293.
40. J. Lin, C. Ma, Q. Wang, Y. Xu, G. Ma, J. Wang, H. Wang, C. Dong, C. Zhang and M. Ding, *Appl. Catal., B*, 2019, **243**, 262-272.
41. W. Zhen, B. Li, G. Lu and J. Ma, *Chem. Commun.*, 2015, **51**, 1728-1731.
42. A. Makdee, P. Kidkhunthod, Y. Poo-arporn and K. C. Chanapattharapol, *J. Env. Chem. Eng.*, 2022, **10**, 107710.